Environmental Earth Sciences (2019) 78:287
https://doi.org/10.1007/s12665-019-8290-4

ORIGINAL ARTICLE

Microscopic structure changes of Malan loess after humidification in South Jingyang Plateau, China

Xiaozhou Zhang[1,2] · Yudong Lu[1,2] · Xin Li[1,2] · Yangchun Lu[1,2] · Wangsheng Pan[1,3]

Received: 28 August 2018 / Accepted: 25 April 2019 / Published online: 6 May 2019

Abstract

As a major engineering material, loess has complex structure and properties. This complexity is manifested in the open metastable packing structure and collapsibility, thereby causing considerable trouble to the environment and human habitation. Several scholars have attempted to reveal the nature of loess. Its structure was investigated using scanning electron microscopy, and the collapsibility was observed in in-suit and laboratory. Results indicate that there is a close relationship between loess collapsibility and structure. Loess collapsibility is the destruction of its metastable structure. Given limited experimental equipment and methods, observing the changes in particle arrangement directly before and after humidification in the same area is difficult. Therefore, the mechanism of loess collapsibility is mainly summarized from experimental observation data or reasonable speculation. In this work, we observed the specific movement and changes of particles in the same area by fixing certain sites in an environment scanning electron microscope of these samples. Six samples were prepared at the beginning of the experiment, and the special sites were fixed at each sample. During the observation we found that three samples could not efficaciously perform micrography efficaciously because the uneven electron conduction excessively brightened the particles to be observed. The three other samples dropped water carefully for humidification in the following 5 days, and the fixed sites were re-observed in the ESEM for the second time. Results showed that loess collapsibility is a macroscopic manifestation under the change in intergranular cementation. In addition, intergranular cement would not completely disappear during once humidification process. By contrast, along with the movement of water, the cement can regroup in an appropriate place and bind the particles until the next humidification process. This condition also causes loess to collapse in every humidification process. This phenomenon has been frequently overlooked by many scholars.

Keywords Loess · Cement · Humidification collapse mechanism · Multi-level collapsibility

Introduction

Loess soils are extensively distributed around the world (Li et al. 2016), and China has the largest loess deposits on earth (Shao et al. 2018; Yuan and Wang 2009; Zhang and Liu 2010). With the improvement of Chinese people's living standard, residents who lived on the Loess Plateau have high requirements on ecological environment construction and living quality. Many scholars have made fruitful achievements in the water quality in the Loess Plateau region (Li et al. 2017, 2018a, b; Wu et al. 2015), but further studies are still needed to study the structural stability of loess; this structural stability is related to the safety of people's life and production. Loess collapsibility is frequently uneven, thereby possibly leading to collapses and landslides at the edge of the plateau; other disasters, including the collapsible pit on the surface of the plateau, have been important problem in the production and living activities of this area (Cheng et al. 2015; Leng et al. 2017; Xu et al. 2012). To reduce the damage caused by collapsibility to engineering and life, many experts and scholars have exerted constant efforts to investigating loess formation and structure; certain approaches have also been summarized to interpret the collapse mechanism of various collapsible soils upon

✉ Yudong Lu
luyudong@chd.edu.cn

[1] College of Environmental Science and Engineering, Chang'an University, Xi'an 710054, China

[2] Key Laboratory of Subsurface Hydrology and Ecology in Arid Areas (Chang'an University), Ministry of Education, Xi'an 710054, China

[3] School of Tourism and Resources Environment, Qiannan Normal University for Nationalities, Duyun 558000, China

humidification; the collapse mechanism, involves the loss of capillary tension (Terzaghi 1943; Xie et al. 2018), solution of soluble salts (Klukanova and Sajgalik 1994), and shortage of clay or bonding materials (Zhang and Qu 2005). These mechanisms have different considerations but are connected and can support on another. Moreover, these theories begin by observing the loess microstructure, i.e., whether the observation method is suitable can considerably affect the analysis of loess microstructure and collapse mechanism.

At present, it is generally accepted that the effective observation of loess microstructure is a variety of the scanning electron microscopes, such as scanning electron microscopy (SEM) (Deng et al. 2010; Jiang et al. 2014; Li and Li 2017), environment scanning electron microscope (ESEM), and focused ion beam scanning electron microscopy (FIB-SEM) (Bultreys et al. 2016; Darbari et al. 2017; Ma et al. 2014). In comparison with an optical microscope (OM), the SEM or ESEM can magnify images to tens of thousands of times, whereas OM is no more than 1000 times. In the SEM field, the resolution is high, and images appear clearer than in OM. Given that SEM can only observe the surface morphology of the samples, nothing can be done for their 3D reconstruction, whereas FIB-SEM shows an advantage in this domain. FIB-SEM can also be used to scan images while using Li-ion beam milling samples and finally obtain 3D data (Taillon et al. 2018). Considering its advantage of 3D reconstruction of scanning data, FIB-SEM is the optimal approach to observing loess microstructure. However, the poor timeliness and expensive price of FIB-SEM in the sample preparation, especially the destruction to the samples, limit the investigation of the humidification and dehumidification deformation of loess on a microscopic scale. Therefore, the samples must be observed before and after humidification twice and must not be damaged. Moreover, the SEM or ESEM image resolution is sufficient for satisfying the requirements of the experiment without considering the 3D reconstruction in order to obtain the surface morphology of the samples. SEM and ESEM remain the most mainstream observation methods and have achieved remarkable results in microstructure study. Through microscopic images, scholars have identified the types of pores (Bai et al. 2015; Lei 1987; Liu et al. 2016), types of particles (Gao 1980; Wang and Ni 2012), the particle connection (Bai et al. 2015; Lei 1983, 1987), and the characteristics of changes in humidification and dehumidification (Jin 2006; Zhang and Zhang 1992; Zhang and Zheng 1990), and the difference between original and compacted loess (Ma et al. 2017; Sun and Matsuoka 2004; Sun et al. 2007).

As the most important collapsible soils, loess is an open metastable packing, and metastability is the main collapsible soils problem (Assadi-Langroudi et al. 2018; Rogers et al. 1994). This metastable structure is determined by loess formation. In the early stage, calcium ions leach from calcite and silicate and enter the uncompacted and loose accumulation dust. Particles with negatively charged and smaller than 5 microns coalesce together to form a group of aggregated particles, for the dust to be initially fixed. During the next process of loessificaion, these aggregated particles and large clastic particles in the dust are cemented again to form a porous structure from the previous low-density deposits. Under the influence of periodic dry–wet alternate continental climate, particles in this porous structure produce connection strength, which gradually turns loose soil into soil with unstable granular overhead structure; this structure is typical for collapsible loess (Gao 1984). When this open metastable structure meets water, the strength of the connection among particles decreases and leads to particle rearrangement; on the macro level, surface subsidence, refers to collapsibility (Barden et al. 1973; Matyas and Radhakrishna 1968; Vanapalli et al. 1999).

As mentioned previously, loess microstructure with humidification and dehumidification was observed through SEM. However, when magnification is large, numerous changes occur in the field of vision, although the samples are slightly moved, finding the same area of interest (AOI) position after the humidification and dehumidification becomes more difficult. Therefore, comparing these SEM images is typically conducted in two different regions. So, comparing the changes in two different regions to sum up the changes in the same area is unreasonable. Therefore, seeking a method to observe the same region before and after humidification is significant. In this work, we achieved this goal by fixing certain sites of the samples. We also obtained the forms of loess deformation and the possibility of multi-level collapsibility.

Study area

Figure 1, illustrates the test site was selected at the cropland between the Provincial Highway S208 and Xiushidu Village (34°29′N, 108°48′E) in Jingyang County, on the south bank of the Jinghe River, South Jingyang Plateau; the plateau is an important part of the Loess Plateau of Weibei (north of Weihe River), with an elevation of 430–500 m and an area of 180 km^2, thus accounting for 23.1% of the total area of this county(Peng et al. 2017).

South Jingyang Plateau is flat and broad and is the most important cultivated land for locals. Jingyang County has warm temperate continental monsoon climate, and the average annual precipitation is 548.7 mm. Nearly all of the precipitation falls from June to September, thereby, indicating that irrigation determines the yield of food. Since the 1970s, people have begun to irrigate their fields on this plateau with water from the Jinghe River to increase food production. With the development of social productivity, the amount of water irrigated in this area has sharply risen. In addition,

Fig. 1 Geographical location of the test site

a series of geological problems have occurred. For example, given perennial irrigation, cropland in this area already exhibits evidence collapsible phenomena, thus resulting in many longitudinal fractures along the river in the Loess Plateau. Such problems have led to the occurrence of a chain of landslides and have continuously reduced arable land as depicted in Fig. 2. The test site is an earth-fetching area. Figure 3 displays that the section of loess from Malan (L_1) to Lower Lishih (L_6) is completely exposed due to artificial cutting. The Malan loess obtained in this site is of Pleistocene age and Aeolian origin upon the earth fetching area.

Method

Sample preparation

To maintain the structural integrity of loess, surface tillage soil and lateral dry floating soil were first removed in the field during the sampling process; after that, the soil sample was cut into 40 $cm^3 \times 40$ $cm^3 \times 40$ cm^3 in situ (see Fig. 3). The cube was then carefully packaged with foam and transported to the laboratory. In the laboratory, the cubic was further cut into several 5 $cm^3 \times 5$ $cm^3 \times 7$ cm^3 pieces and then

Fig. 2 Due to the irrigation, a large amount of water infiltrates into the farmland, resulting in uneven collapse of the land, and longitudinal cracks appear along the edge of the plateau, which reduce the slope stability, leading to the occurrence of landslides

Fig. 3 The section of earth fetching area and test site in Xiushidu village

dried for 12 h in an oven at 104 °C to prepare for the final scanning samples. A trace was carved with a knife on every piece while preparing the scanning samples. The trace must be sufficiently deep to break off every piece with fingers. This treatment could ensure that the sample structure was not damaged, whereas the fresh section could be stereoscopically observed. The soil was trimmed into flake samples with a diameter of 1.0–1.5 cm, and the bottom was polished flat. The surrounding area and the bottom of the scanning samples were fixed with glue. Our goals were (1) to reduce the damage of the loose loess particles in the instrument and (2) to allow a clear line to form between the fixed and non-fixed glue, which is helpful in fixing the AOI. The following conditions were the reasons for selecting the diameter of 1.0–1.5 cm. If the size is smaller than 1.0 cm, then ensuring that adequate fresh sections are available for observation after fixing with glue can be difficult. By contrast, if the size is larger than 1.5 mm, then a rupture may occur within 2 days after fixing with glue. In addition, the later process of humidification and dehumidification could not be achieved.

A total of 14 samples were initially prepared to observe the microstructure and surface morphology of Malan loess. These samples should be observed in SEM twice before and after humidification. Thus, six samples with typical characteristics were selected for observation; that is, Sample 1 and 3 had one or several evident holes distributed in the observation area. Sample 2 was easily distinguished by the observed region boundary. Sample 4 and 5 were aggregates, and Sample 6 had a wormhole in the center position, as demonstrated in Fig. 4. These typical characteristics can divide the observation areas into multiple independent parts to facilitate our positioning or fixing.

Determination of properties

In situ two cutting ring samples with a diameter of 79.8 mm and two cutting ring samples with a diameter of 61.8 mm were prepared to determine collapsibility and permeability coefficients, respectively. The cut soil in soil collecting boxes could be used to measure water content, specific gravity, and other physical properties of loess. In addition, one sample and two parallel samples were prepared to determine the chemical properties of loess, where such properties were averaged from the results of three repeated measurements of each sample. The pH and electrical conductance values of loess were measured by a water quality analysis detector (AZ Instrument AZ-86505). The particle analysis experiment of Malan loess to distinguish the loess grading was determined by the laser particle size distribution instrument (Dandong Bettersize 2000) in the geological engineering laboratory of

Fig. 4 The six samples prepared for observing in SEM. The dark color part was fixed with glue, which is to avoid loose particle pollution of the instrument, and the light color part is the observation area, which was not fixed with glue

Chang'an University. Two samples were selected from different parts of the cube to analyze the grain size. Three sets of repeated experiments were performed for each sample, and three recalculations were performed for each experiment. The final particle analysis was consistent.

Sample marking

As for the loess samples used for scanning, spraying conductive coating for 80 s in the sputter coater (Bal-Tec SCD-005) is necessary for improved observation. To maintain the consistency of the two observation areas and the relative angles before and after humidification, the six samples were fixed with a conductive adhesive on a metal pallet in order. For the convenience of observing the changes in loess microstructure in the same position after humidification, predicting the positions of the potential change during the first observation was required. The typical characteristics of samples provided us with advantages, such as the hole and agglomeration. These typical characteristics were our fixing sites. On the basis of these sites, we could achieve the same location by taking photos continuously on multiple scales, as exhibited in Fig. 5.

Considering the poor loess conductivity, areas that were able to be clearly observed before humidification might be too bright to be observed after humidification. Therefore, when the first SEM scan was conducted in the preliminary stage, the samples should be marked adequately. According to the first images scan and the characteristics of the samples themselves, the same observed areas were found in the second SEM observation. The size, morphology, and connection of the particles were observed again and compared with the first observation results in the image analysis software (Image-Pro Plus).

Humidification and dehumidification processes

The humidification and dehumidification processes of loess were performed immediately after the first SEM observation. Both processes were composed of one humidification process and one dehumidification process. The humidification process comprised multiple water addition processes.

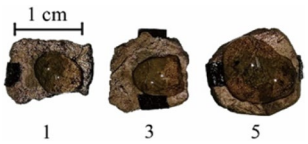

Fig. 6 The samples during humidification

During such processes, the surface of soil samples was wetted by a spray device to eliminate the inhibition effect of the gold coating on water immersion. To confirm if the surface of the samples had changed from golden to dark brown, water was injected on the top of the samples by a 1 ml injector in light contact. That is, by pushing the injector, a small droplet appeared on the needle of the syringe, and then the droplet gently contacted with the surface of the samples. When the droplet touched the surface of the samples, its surface tension was insufficient for supporting its gravity, thus causing the droplet to disperse and all the water acted on the samples. The reason for selecting small droplet in the humidification process was to avoid the impact and destruction of an excessive amount of water on the surface structure of samples after the decrease in the droplet's surface tension. Thus, the principle of low intensity and high frequency should be strictly followed in the water addition process. This process was repeated until a small amount of water accumulated on the surface of the samples. At this point, the water addition process was completed. Simultaneously, the time it took for the surface water of the sample to completely disappear was recorded. Then, the water addition process was repeated until the surface water of the samples disappeared in nearly 30 min. The limited time was within 30 min because the Malan loess samples in Jingyang South Plateau would decompose under the same amount of water without surface gel injection. A total of six water addition processes were conducted in this experiment, which lasted for 5 days. The average water consumption of the samples was 2.7 ml. After completing the humidification process, the samples were naturally dried in the room to achieve the dehumidification process. The humidification and dehumidification processes of loess were then completed. Figure 6 depicts the soil samples during humidification.

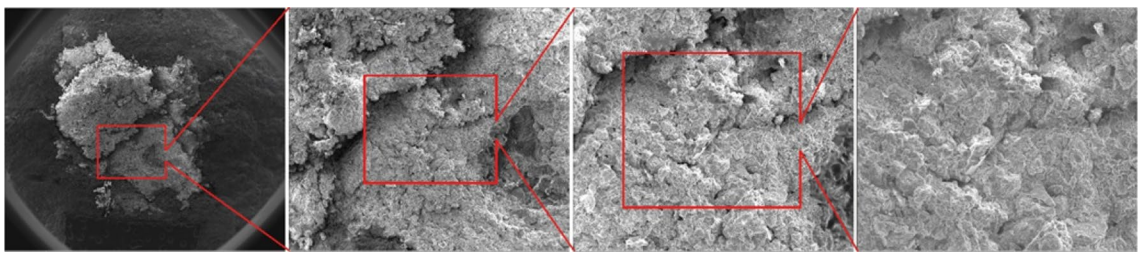

Fig. 5 The method of fixing sites during the observation

Results and discussion

The saltness and concrete gradation of loess are the general and most direct indexes to identify whether loess demonstrates collapsibility. According to the results of particle analysis, we can claim that the loess in this area was well graded and prone to collapse easily. The three main forms of soil particle change can be obtained through image analysis, namely dispersion, dissolution, and reunion.

Physical and chemical properties

By testing the samples and the control group, Table 1 listed the physical and chemical properties of loess.

The results confirm that the data of the two groups of experiments are consistent. The porosity ratio close to 0.8 indicates that the loess in this area is moderately dense and has high porosity, thereby enabling the condition for loess collapse in this area. The relatively favorable permeability ensures that water can quickly go through the pores during the infiltration process and can immediately react with soluble salt. In addition to the physical and chemical properties measured by the samples in cutting rings and soil collecting boxes, two samples were selected from different parts of the cube to analyze the grain size. Three sets of repeated experiments were performed for each sample, and three recalculations were performed for each experiment. The final particle size analysis results reveal that both samples do significantly differ in particle size distribution. Table 2 and Fig. 7 present the results of our report.

Soil uniformity is represented by uniformity coefficient (C_u), and soil gradation continuity is represented by curvature coefficient (C_c). C_u and C_c values are calculated as follows:

$$C_u = \frac{d_{60}}{d_{10}} \quad (1)$$

Table 1 Physical and chemical properties of the loess in in South Jingyang Plateau

Number of samples	PH	Electrical conductance (μs/cm)	Water content (%)	Dry density (g/cm^3)	Specific gravity (G_S)	Porosity ratio (e)	Permeability coefficient (cm/s)	Collapsibility coefficient
1	7.63	592	4.3	1.52	2.741	0.803	1.21E−4	0.035
2	7.60	565	4.2	1.53	2.741	0.792	1.22E−4	0.041

Table 2 The results of particle size analysis of Malan loess (recalculated after the detail report)

Particle Size (μm)	Interval (%)	Cumulative (%)	Particle size (μm)	Interval (%)	Cumulative (%)
0.020–0.039	0	0	6.336–13.11	18.6	42.33
0.039–0.080	0	0	13.11–27.12	26.35	68.68
0.080–0.167	0.71	0.71	27.12–56.13	22.34	91.02
0.167–0.345	1.97	2.68	56.13–116.1	7.86	98.88
0.345–0.715	5.75	7.83	116.1–240.3	1.12	100
0.715–1.479	2.65	10.48	240.3–497.2	0	100
1.479–3.062	2.94	13.42	479.2–1028	0	100
3.602–6.336	10.31	23.73	1028–2000	0	100

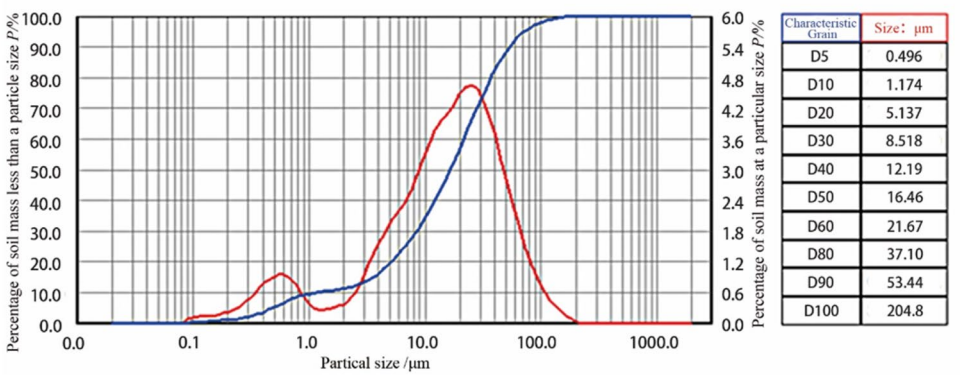

Fig. 7 The distribution curve and cumulative curve of loess grain size and some values of characteristic grain size

$$C_c = \frac{d_{30}^2}{d_{60} \times d_{10}}, \quad (2)$$

where, d_i is the characteristic grain size of soil.

For the Malan loess in Jingyang County, the value of C_u and C_c are 18.46 and 2.85, correspondingly. Therefore, the loess in this area is graded with continuity and non-uniformity. However, from an engineering perspective, this soil is well graded ($C_u \geq 5$, $C_c = 1$–3). The fine particles filling the pores formed by coarse particles can easily obtain high dry density, high porosity, and improved mechanical properties, which can easily collapse after humidification. Therefore, the loess in South Jingyang Plateau is collapsible during irrigation.

Image analysis

After conducting the laser particle size analysis in our study site, two SEM image observations are closely followed. In the first SEM observation, the microstructure, particle morphology, and particle contact of the six samples are observed. Multiscale photographs of the specific parts in the microscopic fields and the possible place to change in prediction are considered to quickly find the same area in the second observation. Given the poor loess conductivity, the problem of uneven electrical conductivity still exists, although the surface of samples already has a conductive coating. Thus, only three samples can satisfy the requirements of the second observation (i.e. Samples 1, 3 and 5).

Particle types of the Malan loess

Similar to the results of previous studies, the particle of Malan loess is composed of sand, silt, and clay. Table 2 lists that, in South Jingyang Plateau, the content of sand grains is relatively low, accounting for approximately 8% of the total mass. By contrast, silt occupies the dominant position. Its quality score is 80%, and the content of the clay is approximately 12%.

Figure 8 illustrates that sand and silt are mainly block and flake-shaped, respectively. The flaky particles have a flat surface and neat edge with an uneven fracture, whereas blocky particles are the opposite. Their surface is rough, their edges are not neat, and they have a hackly fracture. Nearly all of the flaky particles are horizontally stacked, except for a few particles that are inserted into the spaced or intergranular pores, which are formed by the two types of particles.

In contrast to the pores that are only formed by flaky particles, those formed by blocky particles are increasingly unstable because, when block particles are in contact with other particles, they have a tilt angle, which is different from flaky particles. Clay acts as a filling and bonding material between sand and silt. In contrast to the two other types of particles, the clay morphology is similar to a polyhedral structure, which consists of three forms, namely aggregate, sub-angular blocky, and lump. Figure 8 demonstrates that silt particles are clothed in clay plates. In addition, spaced and intergranular pores are filled with clay particles, which combine the sand and silt, strengthen the connection among particles, and build the overall structure. Other clay particles adhered to the sand or silt surface can combine until another particle(s) is(are) added.

As for the 3 samples, 26 images of the 11 same regions are identified to analyze the microstructure changes. Each sample is separately analyzed. Markings on the images are essentially of two types, in which circles were used to indicate the apparent changes in particles in the images. Moreover, polygons represent areas where significant changes have occurred.

Sample 1

The particles of Sample 1 are mainly silt and the size is basically between 20 and 40 μm, which is the largest number of particles in this region. The number of blocky particles is larger than that of flaky particles.

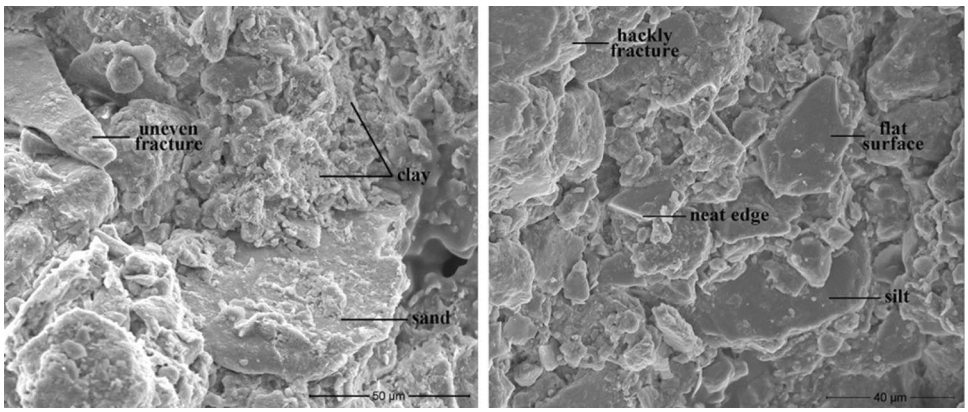

Fig. 8 The types of particle and fracture of Malan loess

By comparing Fig. 9a, b, a narrow and discontinuous "crack" changes into a wide and continuous "crack" along the northeast direction in the center of the image after humidification. A mass of particles, such as C4 and C6, are dropped into the "crack" and have shifted certain angles. In addition to certain particles that filled the pores in the "cracks", other particles are stacked with large particles. When clay particles exist, the silt particles are cemented together to enhance the structural stability of the loess again. The same case has occurred in A1 and C1 areas. Another case is the movement of single particles, such as C3 and A2. Blocky particles move from the C3 position (Fig. 9a) to the C2 position (Fig. 9b) during the humidification and dehumidification processes. A blocky particle is observed in the A2 area, which is not found before humidification. These particles are not closely related to the particles that they were in contact with. Therefore, they are unstable and will move again with subsequent vibrations or humidification process. The particle morphology change in the C5 position (Fig. 10) is the third kind of loess microstructure change called the "dissolution" of a particle.

Such dissolution has occurred in the area indicated by red arrows. The maximum Feret diameter of the front end of the particle is changed from 27.5 to 20 μm, thereby indicating that a considerable amount of silt has been dissolved into clay with water. If the clay is in contact with sand or silt, then the clay will act as a cohesive force and stick the scattered particles into a whole. Particle change is a continuum of dissolution and reunion, thus continuously occurring.

Sample 3

The particles of Sample 3 are dominated by closely aligned flaky sand. Intergranular pores, such as the area under C1, are approximately 5 μm. The spaced pores in the C2 position and the center of the image are formed by few blocky particles. Notably, the particles in C1 have changed during the first scan process. In contrast to other particles, changes have occurred under the moisture of water.

Different from Sample 1, the cracks in the middle of Sample 3 are not vertical but oblique after humidification. The preliminary judgment is that the flaky particles were arranged in layers, and when the water was encountered, the squeezing of particles and the buoyancy of water have led to the upward arch of the upper layer. Considering the loss of support, the spaced pores in C2 and C3 collapsed and their particles dispersed. The scattered particles also remain in their original shape but vary in angle.

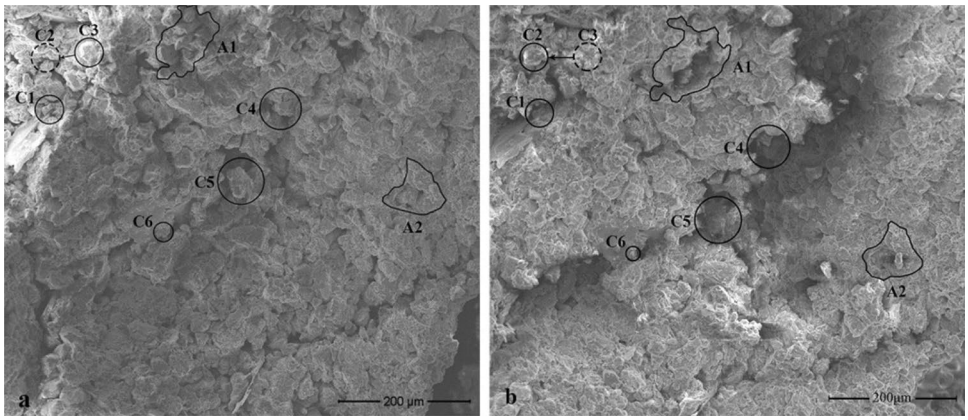

Fig. 9 **a** The microstructure of sample 1 before and **b** after the humidification

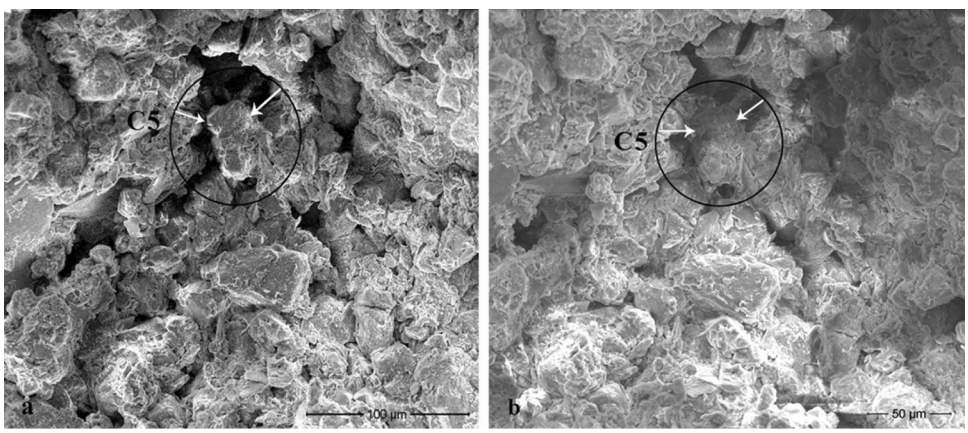

Fig. 10 The "dissolution" of silt particle at C5 position

In the magnification depicted in Fig. 11, no evident morphological changes are observed at the C1 position. However, when the magnification was further enlarged, changes have appeared in this region (for detailed information about the changes, see Fig. 12). A particle in the C4 area has disappeared, and another particle has an evident downward movement. The porosity among the particles is larger in Fig. 12b than in Fig. 12a. In addition, the particles are dispersed in Fig. 12b; this finding can also be certified from the images at the C5 position. The image of C5 is brighter in Fig. 12b than in Fig. 12a indicating that the particles disperse further after infiltration, and conductivity worsens. Therefore, many electrons are gathered, thereby causing the image to be highlighted here.

Sample 5

In contrast to the two previous samples, changes in the microstructure of Sample 5 are shown in the aggregates. On the one hand, the bond among aggregates decreases rapidly after infiltration, thus separating the originally contacted aggregates and widening the gaps. On the other hand, the aggregates with an empty face, such as C2 and C4, are most likely to be destroyed. The particles in C2 disperse and fall to the crack (Fig. 13b) in C3, given water and gravity. Moreover, the bond strength among the silt in C4 decreases with the reduction in clay. Thus, the stability of the aggregate structure is weakened, and a great risk of disintegration is observed in the next humidifying process. Moreover, organic matter degradation plays an important role in the loess microstructure. For example, turf degradation in C1 can affect the connection between particles and structure stability.

In organic matter degradation, grass or turf can be broken into sections or small pieces. Both can also play an important part in adsorption or bonding. Figure 14b, illustrates that the silt or clay is attached to the broken turf in C6. Furthermore, in C5, the silt that moved from another place will be similarly attached to the turf in the future humidification process. The turf in C6 may

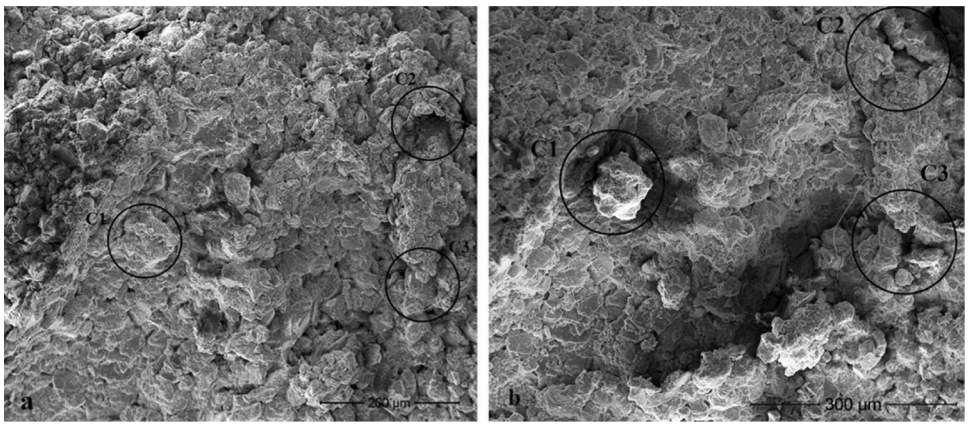

Fig. 11 **a** The microstructure of sample 3 before and **b** after the humidification

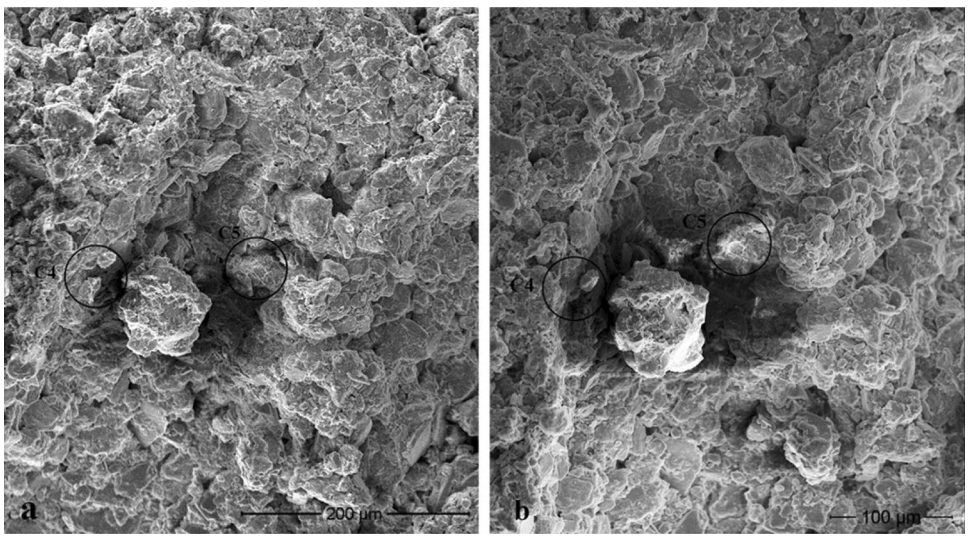

Fig. 12 The details of the microstructure at C1 position

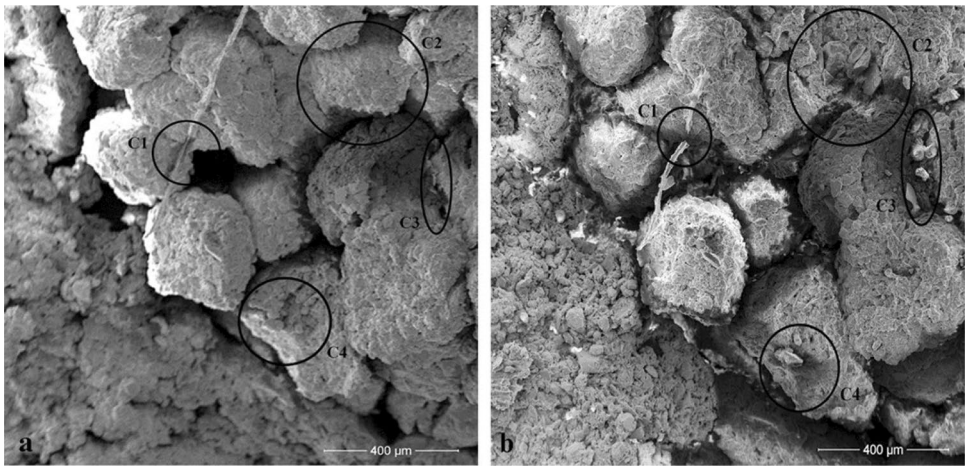

Fig. 13 The changes of microstructure of sample before and after the humidification of sample 5

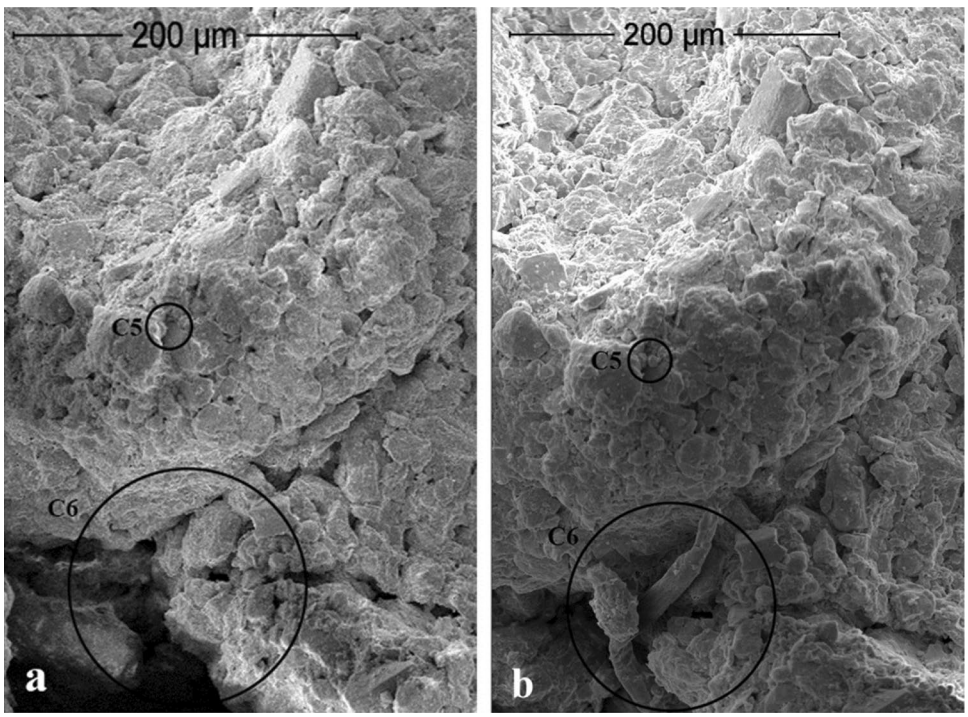

Fig. 14 The changes of microstructure of sample before and after the humidification of sample 5

form a new aggregate or may be further degraded with the increase in infiltration. These different results lead to diametrically opposed conclusions. On the one hand, the aggregate form can enhance the contact among particles and stability of localized areas, but can worsen the overall structural integrity. On the other hand, the overall structural integrity of loess will be enhanced, because further degraded organic matter and clay are re-cemented in the small pores. This dynamic cycle also leads to the continuity of loess structure change, which eventually leads to multi-collapsibility.

Mechanical analysis

Through the analysis and summary of the three types of loess particles and pore characteristics, we claim that the collapsibility mechanism of loess follows traditional catastrophe theory. However, certain differences are identified. Similar to the traditional viewpoint, the connection among loess particles (i.e. cementation) is closely related to their water content, which is expressed by spring stiffness coefficient (k_W) related to saturation in catastrophe theory. This theory regards loess collapsibility as a dynamic process. In

contrast to the traditional one, loess particles cannot be simply regarded as a rigid sphere, and the connection among particles cannot be simply regarded as a ball–stick relationship. Soluble types of cement wrapped among particles or around particles themselves can dissolve with water. Therefore, the pore structure is destroyed. With the decrease in water content, cement, and other substances, filling pores with dispersed particles can re-aggregate and form a part of spaced pores again, thus providing conditions for further collapsibility. Therefore, loess collapsibility process is a cyclic process of damage–healing–damage, not a single process.

Conclusion

The following conclusions can be drawn from this work:

1. As the main constituents of loess in Jingyang County, the two forms of silt morphology constitute two distinct structures of loess. These structures lead to different deformations during the humidification process. Blocky particles can easily form a structure with high spaced pores and intergranular pores. When the water is humidified, a crack can be formed along the original crack or the weak spot where the collapse mainly occurs. Given the tight horizontal arrangement of flaky particles, the spaced pores and cracks rarely appear in this area, and the deformation of this area subsides.
2. Deformation is expressed as an aggregate decomposition. Decomposed aggregates may form new aggregates or further decompose into silt and clay.
3. Different deformation forms and structures result in an uneven collapse of the entire loess microstructure.
4. Although the three types of morphological deformation are different, they are individually accompanied by the newly formed open metastable packing structure, rather than the stable state. Therefore, the collapsibility of the Malan loess can be rediscovered during the subsequent humidification process, and the cycle cannot terminate.

These conclusions may be valuable for further understanding the collapsibility during the humidification process. In addition, the types of cementation among the loess particles on loess collapsibility are also important. Such types are the focus of our next study on the water-physical property of nature loess.

Acknowledgements This work was financially supported the Key program of National Natural Science Foundation of China (Grant No. 41630634) and the Innovation Group and Major Research Project of the Education Department of Guizhou Province (Grant No. QJH-KY [2016]054, QJH-KY [2016]055).

References

Assadi-Langroudi A, Ng'ambi S, Smalley I (2018) Loess as a collapsible soil: some basic particle packing aspects. Quatern Int 469:20–29. https://doi.org/10.1016/j.quaint.2016.09.058

Bai XH, Ma FL, Wang M, Jia JG (2015) Micro-structure and collapsibility of loess in China. Crc Press-Taylor & Francis Group, Boca Raton

Barden L, McGown A, Collins K (1973) The collapse mechanism in partly saturated soil. Eng Geol 7:49–60

Bultreys T, De Boever W, Cnudde V (2016) Imaging and image-based fluid transport modeling at the pore scale in geological materials: a practical introduction to the current state-of-the-art. Earth-Sci Rev 155:93–128. https://doi.org/10.1016/j.earscirev.2016.02.001

Cheng YX, Huo AD, Zhang J, Lu YD (2015) Early warning of meteorological geohazard in the Loess Plateau: a study in Huangling County of Shaanxi Province in China. Environ Earth Sci 73:1057–1065. https://doi.org/10.1007/s12665-014-3455-7

Darbari Z, Jaradat KA, Abdelaziz SL (2017) Heating-freezing effects on the pore size distribution of a kaolinite clay. Environ Earth Sci 76:8. https://doi.org/10.1007/s12665-017-7069-8

Deng J, Wang LM, Zhang ZZ, Bing H (2010) Microstructure characteristics and forming environment of late quaternary period loess in the loess plateau of China. Environ Earth Sci 59:1807–1817. https://doi.org/10.1007/s12665-009-0162-x

Gao GR (1980) The microstructure of loess in China. Chin Sci Bull 25:945–948 **(in Chinese)**

Gao GR (1984) Microstructure of loess soil in China relatiive to geographic and geology environment. Acta Geol Sinica 58:265–270 **(in Chinese)**

Jiang MJ, Zhang FG, Hu HJ, Cui YJ, Peng JB (2014) Structural characterization of natural loess and remolded loess under triaxial tests. Eng Geol 181:249–260. https://doi.org/10.1016/j.enggeo.2014.07.021

Jin MX (2006) Effects of moistening and demoistening of collapsible loess. Geotech Eng Tech 20:203–207 **(in Chinese)**

Klukanova A, Sajgalik J (1994) Changes in loess fabric caused by collapse: an experimental study. Quat Int 24:35–39. https://doi.org/10.1016/1040-6182(94)90036-1

Lei XY (1983) The type of microstructure of loess in Xi'an. JNWU 13:56–65; 127–132 **(in Chinese)**

Lei XY (1987) The pore type and collapsibility of loess in China. Sci Sin (episodes B) 17:1309–1318 **(in Chinese)**

Leng YQ, Peng JB, Wang QY, Meng ZJ, Huang WL (2017) A fluidized landslide occurred in the Loess Plateau: a study on loess landslide in South Jingyang tableland. Eng Geol 236:129–136. https://doi.org/10.1016/j.enggeo.2017.05.006

Li XA, Li LC (2017) Quantification of the pore structures of Malan loess and the effects on loess permeability and environmental significance, Shaanxi Province, China: an experimental study. Environ Earth Sci 76:14. https://doi.org/10.1007/s12665-017-6855-7

Li P, Vanapalli S, Li TL (2016) Review of collapse triggering mechanism of collapsible soils due to wetting. J Rock Mech Geotech Eng 8:256–274. https://doi.org/10.1016/j.jrmge.2015.12.002

Li PY, He S, He XD, Tian R (2017) Seasonal hydrochemical characterization and groundwater quality delineation based on matter element extension analysis in a paper wastewater irrigation area, Northwest China. Expos Health 9:1–18. https://doi.org/10.1007/s12403-017-0258-6

Li PY, He X, Li Y, Xiang G (2018a) Occurrence and health implication of fluoride in groundwater of loess aquifer in the Chinese Loess Plateau: a case study of Tongchuan, Northwest China. Expos Health. https://doi.org/10.1007/s12403-018-0278-x

Li PY, Qian H, Wu J (2018b) Conjunctive use of groundwater and surface water to reduce soil salinization in the Yinchuan Plain,

North-West China. INT J Water Resour D 34:337–353. https://doi.org/10.1080/07900627.2018.1443059

Liu Z, Liu FY, Ma FL, Wang M, Bai XH, Zheng YL, Yin H, Zhang GP (2016) Collapsibility, composition, and microstructure of loess in China. Can Geotech J 53:673–686. https://doi.org/10.1139/cgj-2015-0285

Ma Y, Zhong NN, Huang XY, Guo ZP, Yao LP (2014) The application of focused ion beam scanning electron microscope (FIB-SEM) to the nanometer-sized pores in shales. J Chin Electron Microsc Soc 33:251–256 **(in Chinese)**

Ma FL, Yang J, Bai XH (2017) Water sensitivity and microstructure of compacted loess. Transp Geotech 11:41–56. https://doi.org/10.1016/j.trgeo.2017.03.003

Matyas EL, Radhakrishna HS (1968) Volume Change Characteristics of Partially Saturated Soils. Géotechnique 18:432–448. https://doi.org/10.1680/geot.1968.18.4.432

Peng JB, Wang GH, Wang QY, Zhang FY (2017) Shear wave velocity imaging of landslide debris deposited on an erodible bed and possible movement mechanism for a loess landslide in Jingyang, Xi'an, China. Landslides 14:1503–1512. https://doi.org/10.1007/s10346-017-0827-6

Rogers CDF, Dijkstra TA, Smalley IJ (1994) Hydroconsolidation and subsidence of loess Studies from China, Russia, North America and Europe. Eng Geol 37:83–113

Shao X, Zhang H, Tan Y (2018) Collapse behavior and microstructural alteration of remolded loess under graded wetting tests. Eng Geol 233:11–22. https://doi.org/10.1016/j.enggeo.2017.11.025

Sun DA, Matsuoka H (2004) Collapse Behavior of Compacted Clays in Suction-Controlled Triaxial Tests. Geotech Test J 27:362–370. https://doi.org/10.1520/GTJ11418

Sun DA, Sheng D, Xu Y (2007) Collapse behaviour of unsaturated compacted soil with different initial densities. Can Geotech J 44:673–686

Taillon JA, Pellegrinelli C, Huang Y-L, Wachsman ED, Salamanca-Riba LG (2018) Improving microstructural quantification in FIB/SEM nanotomography. Ultramicroscopy 184:24–38. https://doi.org/10.1016/j.ultramic.2017.07.017

Terzaghi K (1943) Theoretical soil mechanics. Wiley, New York

Vanapalli SK, Fredlund DG, Pufahl DE (1999) The influence of soil structure and stress history on the soil–water characteristics of a compacted till. Geotechnique 51:573–576. https://doi.org/10.1680/geot **(1999.49.2.143)**

Wang HN, Ni WK (2012) Quantitative analysis of loess microstructure based on CT and SEM images. Rock Soil Mech 33:243–248 **(in Chinese)**

Wu JH, Li PY, Qian H (2015) Hydrochemical characterization of drinking groundwater with special reference to fluoride in an arid area of China and the control of aquifer leakage on its concentrations. Environ Earth Sci 73:8575–8588. https://doi.org/10.1007/s12665-015-4018-2

Xie W, Li P, Vanapalli SK, Wang J (2018) Prediction of the wetting-induced collapse behaviour using the soil-water characteristic curve. J Asian Earth Sci 151:259–268. https://doi.org/10.1016/j.jseaes.2017.11.009

Xu L, Dai FC, Gong QM, Tham LG, Min H (2012) Irrigation-induced loess flow failure in Heifangtai Platform, North-West China. Environ Earth Sci 66:1707–1713. https://doi.org/10.1007/s12665-011-0950-y

Yuan ZX, Wang LM (2009) Collapsibility and seismic settlement of loess. Eng Geol 105:119–123. https://doi.org/10.1016/j.enggeo.2008.12.002

Zhang M, Liu J (2010) Controlling factors of loess landslides in western China. Environ Earth Sci 59:1671–1680. https://doi.org/10.1007/s12665-009-0149-7

Zhang YS, Qu YX (2005) Cements of sand loess and their cementation in North Shaanxi and West Shanxi. J Eng Geol 13:18–28. https://doi.org/10.3969/j.issn.1004-9665.2005.01.003 **(in Chinese)**

Zhang SM, Zhang W (1992) The collapsibility of loess during humidification and dehumidification. Chin J Geotech Eng 14:57–61 **(in Chinese)**

Zhang SM, Zheng JG (1990) The deformation characteristics of collapsible loess during moistening process. Chin J Geotech Eng 12:21–31 **(in Chinese)**